RESEARCH ARTICLE | APRIL 17 2024

Quantum sensing effect of electron tunneling in DQD/analyte complex

I. Filikhin ; B. Vlahovic ; A. Joseph ; T. Alston ; J. Oxley

AIP Advances 14, 045230 (2024)
https://doi.org/10.1063/5.0191098

Quantum sensing effect of electron tunneling in DQD/analyte complex

Cite as: AIP Advances 14, 045230 (2024); doi: 10.1063/5.0191098
Submitted: 19 December 2023 • Accepted: 2 April 2024 •
Published Online: 17 April 2024

I. Filikhin,[1,a)] B. Vlahovic,[1] A. Joseph,[1] T. Alston,[1] and J. Oxley[2]

AFFILIATIONS

[1] CREST, North Carolina Central University, Durham, North Carolina 27707, USA
[2] Department of Chemical Engineering, University of Rhode Island, Kingston, Rhode Island 02881, USA

[a)] **Author to whom correspondence should be addressed:** ifilikhin@nccu.edu

ABSTRACT

We investigate electron tunneling between quantum dots and molecules to propose a quantum sensor. This sensor consists of double quantum dots (DQD) with energy levels specifically tailored to mirror those of the target analyte. By analyzing the spectral distribution of electron localizations in the DQD system, we can delineate the analyte's spectrum and deduce its composition by comparing it with a reference sample. To understand electron tunneling dynamics within the DQD/analyte complex, we performed three-dimensional computational modeling applying the effective potential approach to the InAs/GaAs heterostructure. In this modeling, we mimicked the analyte spectrum by utilizing a quantum well characterized by a quasi-discrete spectrum. Our calculations reveal the inherent potential of utilizing this method as a highly sensitive and selective sensor.

I. INTRODUCTION

Electron tunneling between quantum dots (QD) and molecules has generated significant interest in the field of nanosensors and nanotechnology. This process involves the transfer of electrons across a potential barrier, allowing for the exchange of charge and energy between the quantum dots and the molecules in its vicinity.[1–6] It is well known that the tunneling process in nano-scaled systems is highly sensitive to the inter-dot distance[7–9] and energy alignment between the confinements of subsystems. The similar effect takes place in the case of tunneling in a QD/molecule system. The separation and energy alignment can significantly change the tunneling probability. This allows to utilize electron tunneling as a sensitive mechanism for detecting molecules in such quantum sensors.

Furthermore, electron tunneling can be modulated by external factors such as temperature, pressure, and applied electric or magnetic fields. This tunability allows for the manipulation and control of electron transfer processes, enabling the design of novel sensing platforms and devices.[10] By engineering the properties of the quantum dots and the surrounding molecules, the tunneling characteristics can be tailored to enhance sensitivity and selectivity in detecting target molecules.

The study of electron tunneling between quantum dots and molecules holds immense potential for various applications. It has been utilized in fields such as molecular electronics, chemical sensing, and single-molecule detection. By harnessing the principles of quantum mechanics and the intricate interplay between electrons and molecules, continually advance our understanding and harness the unique capabilities of electron tunneling for a wide range of scientific and technological advancements.

An example of electron tunneling between quantum dots and molecules occurs in scanning tunneling microscopy (STM). In STM, a sharp tip is brought into close proximity to the surface of a sample, which may contain a quantum dot and surrounding molecules. By applying a voltage between the tip and the sample, electrons can tunnel between them, resulting in a measurable tunneling current. The magnitude of this current is influenced by the electronic properties of the molecules and the quantum dot, enabling the characterization and identification of specific molecules.

The tunneling current in STM experiments offers valuable insights into the electronic structure, energy levels, and spatial

charge distribution within the molecules and the quantum dot. Variations in the tunneling current can indicate the presence of particular molecules, their binding to the quantum dot, or even their chemical reactions on the surface. Through careful analysis of the tunneling behavior, it is possible to gain an understanding of the nature of the molecules and their interactions with the quantum dot. However, it is important to note that it is not practical to use STM as a quantum sensor. Detection of tunneling between a quantum dot and an analyte can be accomplished through various indirect methods. Some of them are described in the review,[11] which examines the interaction of colloidal quantum dots with molecules. It is essential to highlight that these studies are experimental in nature.

The properties of electron tunneling behavior through individual molecules and a binary nanostructure have been examined in Refs. 12 and 13, wherein electron transport was characterized within the terminology of thermoelectricity. These studies also incorporated vibrational modes for molecules.

In our current study, we have directed our attention toward quantum dot sensing utilizing a semiconductor structure, as detailed in Ref. 14. The confinement of quantum dots results in discrete energy levels for electrons, akin to the energy levels observed in atoms. Within a double quantum dot (DQD) configuration, electrons have the ability to tunnel through the potential barrier between the DQD structures and the surrounding medium. The primary objective of our project is a computational investigation of electron coupling between the molecular states of an analyte and the confinement levels of the semiconductor DQD. We aim to elucidate the mechanism of resonance coupling utilizing the two-level theory, as referenced in Ref. 15. Essentially, coupling occurs in situations where levels undergo anti-crossing.

The detection of electron tunneling between two coupled quantum dots typically entails employing various experimental techniques, such as Coulomb Blockade analysis,[16–18] Transport Spectroscopy,[19–21] and Single-Electron Transistor measurements.[22] Employing a combination of these experimental methods, along with meticulous device fabrication and control, enables the detection and characterization of electron tunneling between coupled quantum dots within a double quantum dot system.

Examples of potential sensors utilizing a double quantum dot can be found in the literature. These sensors can be categorized as follows: (a) Electric field sensors: The tunneling current between the two quantum dots in a DQD is sensitive to the electric field in their vicinity, as the energy levels of the electrons in the dots are influenced by the electric field. Variations in the tunneling current can thus be utilized to gauge the strength of the electric field.[23–25] (b) Magnetic field sensors: The tunneling current between the two quantum dots in a DQD is responsive to the magnetic field in their vicinity since the spin of the electrons in the dots is influenced by the magnetic field. Alterations in the tunneling current provide a means to measure the magnetic field strength.[26] (c) Temperature sensors: The tunneling current between the two quantum dots in a DQD is sensitive to the environmental temperature, as the temperature affects the energy levels of the electrons in the dots. Changes in the tunneling current enable the measurement of the ambient temperature.[27] (d) Biosensors: The tunneling current between the two quantum dots in a DQD can be employed to detect the presence of biomolecules, as these molecules can impact the energy levels of the electrons in the dots. Fluctuations in the tunneling current allow for the measurement of biomolecule concentration in the environment.[28,29] The aforementioned papers are pertinent to our work because they utilize DQDs as the sensing component of a sensor. However, our specific study involves an array of DQDs interacting with analyte molecules via resonance tunneling over a barrier to emulate the spectral characteristics of the analyte for comparison with a reference. The array of DQDs enables precise measurements for detailed comparison purposes.

Generally, the investigation of tunneling between quantum dots and molecules represents a highly promising avenue for advancing quantum device technology. This area of research holds significant potential because it enables the deliberate coupling of electron levels across distinct structures, offering the opportunity to engineer novel functionalities in quantum computing, sensing, and communications.

II. ELECTRON SPECTRA OF DQD AND ANALYTE

We assume that both the DQD and the analyte have discrete spectra, particularly at low temperatures where quantum electron levels manifest a distinctly discrete structure. We posit that the DQD exhibits such a discrete spectrum, with the simplest configuration of

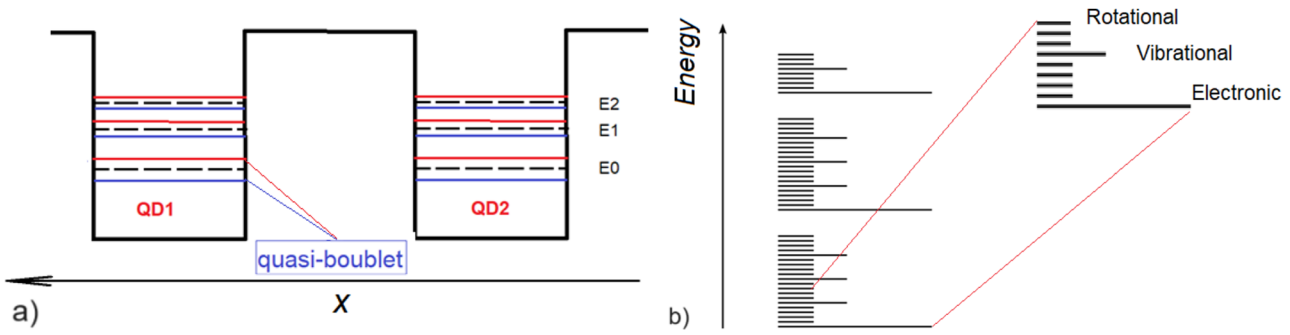

FIG. 1. (a) The electron spectra (E_0, E_1, E_2) of uncoupled identical quantum dots (QD1 and QD2) within a one-dimensional model are depicted by dashed lines. The solid lines represent the coupled states forming quasi-doublets in the DQD. The horizontal axis denotes the spatial coordinate, represented by x. (b) The schematic representation of a molecular electronic spectrum.

the DQD spectrum presented in Fig. 1(a), which corresponds to a DQD comprising two identical quantum dots. The coupling between quantum dots in the DQD leads to the splitting of each electron level of the individual QD to double levels (quasi-doublets). It is noteworthy that a conceptual analogy can be drawn: the quasi-doublet corresponds to the bonding and antibonding molecular states found in diatomic molecules.

The temperature effects give rise to a quasi-discrete spectrum for the molecules of the analyte. The spectrum of a molecule is schematically shown in Fig. 1(b). At room temperature, thermal effects can also play a role in broadening the energy levels and introducing additional thermal excitations. This broadening can result in a smearing of the discrete energy levels and the formation of a quasi-continuous spectrum.

The electron levels are accompanied by rotational and vibrational levels.[30] It is well known that the coupling in different parts of the spectrum has a complex character. One can find examples of vibronic coupling in molecules and phonon coupling in solids in Refs. 31 and 32. The spacing between vibrational and rotational energy levels is generally much smaller than electronic energy level differences. As a result, vibrational and rotational transitions typically occur at lower energies (infrared and microwave regions) compared to electronic transitions that appear within visible and ultraviolet regions.

We consider electron tunneling between the analyte molecular states and the confinement levels of a semiconductor quantum dot as the foundation for a quantum sensor. The quantum sensor comprises an InAs/GaAs double quantum dot designed to detect an analyte. To emulate the spectrum of the analyte, we employ an InAs/GaAs quantum well (QW) positioned adjacent to the DQD. Therefore, our focus is on resonance tunneling in a three-dimensional (3D) nano-scaled InAs/GaAs DQD/QW complex with a mixed spectral structure: a discrete spectrum for QDs and a quasi-discrete spectrum for QW. It is worth noting that tunneling effects in the QD/QW complex were recently modeled in Ref. 8 for a 2D geometry.

The single electron wave function may be localized in the QW (or in the DQD) or delocalized when it is spread over the whole system. The two-level system theory describes the dynamics of the localized/delocalized states in the system. The influence of the quantum well could change localized/delocalized states in DQD to different degrees for different parameters of QW (analyte). In this modeling, we consider localized/delocalized states in the DQD as a tool to detect an analyte. The targeting parameter is the dynamics of electron tunneling within DQD, depending on changes in the QW. Thus, the tunneling between DQD detects the specific QW confinement (material of an analyte).

Input parameters of the model for the complex can be chosen according to the typical sizes of InAs/GaAs dots reported in the literature.[33] The geometry of the DQD and DQD/QW complex is shown in Fig. 2. The QDs have spheroidal shapes with different radial sizes. The material of the DQD was chosen to be InAs. We assume that the DQD is embedded into a GaAs substrate. The boundary conditions (BCs) for the QW along the x-axis are Neumann BCs. On other boundaries, the Dirichlet BCs are satisfied. The spectral distribution of the energy levels of a single electron in a quantum well can be explained by the electron spectra of the quantum box.

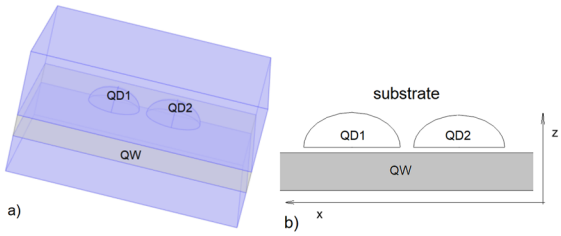

FIG. 2. (a) The 3D geometry of the DQD/QW complex including left quantum dot (QD1), right quantum dot (QD2), and quantum well (QW). The sizes of the QDs can be different based on experimental conditions and material properties. (b) The cross-section of the complex.

The approximation can be written as follows: $E_{nlm} \sim \left(\frac{n^2}{d_x^2} + \frac{m^2}{d_y^2} + \frac{p^2}{d_z^2}\right)$, where $n, m, p = 0, 1, 2, \ldots$ and d_x, d_y, d_z are the sizes of the QW along the respective axes. The main points of interest are a non-linear distribution of energies in the spectrum and covering the spectra with different distributions related to different sizes.

III. InAs/GaAs QD AND QW: EFFECTIVE POTENTIAL MODEL

We consider quantum dots composed of InAs in a GaAs substrate. This heterostructure is modeled[34] utilizing a ***kp***-perturbation single subband approach. The problem is mathematically formulated by the Schrödinger equation in three dimensions (3D),

$$\left(\hat{H}_{kp} + V_c(r) + V_s(r)\right)\Psi(r) = E\Psi(r). \quad (1)$$

Here, $\hat{H}_{kp}$ is the single band ***kp***-Hamiltonian operator $\hat{H}_{kp} = -\nabla\frac{\hbar^2}{2m^*}\nabla$, $m^* = m^*(r)$ is the electron effective mass, which depends on the position of the electron, and $V_c(r)$ is the bandgap potential. $V_c(r) = 0$ inside the QD and is equal to V_c outside the QD, where V_c is defined by the conduction band offset for the bulk. The bandgap potential for the conduction band is chosen as $V_c = 0.594$ eV. Bulk effective masses of InAs and GaAs are $m_1^* = 0.024m_0$ and $m_2^* = 0.067m_0$, respectively, where m_0 is the free electron mass. $V_s(r)$ is the effective potential simulating the strain effect, it has an attractive character and acts inside the volume of the QD.[34] The magnitude of the potential can be chosen to reproduce experimental data. For example, the magnitude of V_s for the conduction band chosen in Ref. 35 is 0.31 eV according to the comparison to the experimental data.

IV. ELECTRON TUNNELING IN DQD

To describe the tunneling of a single electron in a double quantum dot, we make the following definitions. Probability of localization of electron into region Ω_y ($y = 1,2$) is defined as $N_{k,y} = \int\int\int_{\Omega_y} |\Phi_k(x,y,z)|^2 dxdydz$, where $\Phi_k(x,y,z)$ is the wave function of electron, $k = 1, 2, \ldots$ enumerates the levels in the spec-

trum. Ω_γ ($\gamma = 1, 2$) are concurred with the QD shapes. Let us define the tunneling measure parameter,

$$\sigma = \frac{N_{k,1} - N_{k,2}}{N_{k,1} + N_{k,2}}, \tag{2}$$

in the range of $[-1, 1]$. Obviously, when $\sigma = 0$, the electron will be in QD1 (Ω_1) or QD2 (Ω_2) with equal probability (here, we assume that the QD1 and QD2 have the same shape). We will call this electron state the delocalized state of an electron in a DQDs system. Case $\sigma = 1$ (or $\sigma = -1$) corresponds to the strong localization of a single electron in QD1 (or QD2).

Another method to analyze the electron localization and spectral distributions of localized/delocalized states is based on an evaluation of the averaged z coordinate of electron in the complex as a binary system of the DQD and the analyte. Let us consider electron levels in 1D bi-confinement potential shown in Fig. 1(a) with the energies $E^{(n)}$, $n = 1, 2, 3, \ldots$ listed in increased order of energy values. The model utilizes the coupling parameter, Θ, which defines the delocalized ($\Theta \approx \frac{\pi}{2}$) and localized ($\Theta \approx 0$) states of a single electron. This parameter depends on $\Delta^{(n)}$, the difference between energy levels of the left and right QDs, the considered spectra are those of separated QDs. In this study, the difference is caused by a shape symmetry breaking. For a one-dimensional two-level system, the dependence of the localization of a single electron in DQD may be expressed[15,36] by the ratio $W^{(n)}/\Delta^{(n)}$, where W^n is defined by the wave functions overlap for separated QDs and $\Delta^{(n)}$ is the energy difference between n-th electron levels in the spectra of separated QDs,

$$\Theta^{(n)} = \arctan\left(2W^{(n)}/\Delta^{(n)}\right), \; n = 1, 2, 3, \ldots. \tag{3}$$

Here, the delocalized state corresponds to a coupling in the QDs. The wave functions of each level [the spectral quasi-doublet, shown in Fig. 1(a)] can be expressed as follows:

$$\Psi_+ = \psi_0 + \tan(\Theta/2)\psi_1, \qquad \Psi_- = -\tan(\Theta/2)\psi_0 + \psi_1,$$

where the normalizing constant is arbitrary. The wave functions of the unperturbed states are noted for ψ_0 and ψ_1 and indexed by 1 or 2 for separated left and right quantum wells, respectively. For identical QDs in DQD, each unperturbed energy level splits into two. To analyze the electron localization, we calculate the single electron average coordinate $\langle x \rangle$, calculated as matrix elements,

$$\langle x \rangle_i = \langle \psi_i | \, x \, | \psi_i \rangle, \quad \langle x \rangle_{ij} = \langle \psi_i | \, x \, | \psi_j \rangle, \quad i, j = 0, 1,$$

which are associated with the electron wave functions $|i\rangle$ in QD1 and QD2, respectively, which are considered separately. The x-coordinate origin is chosen to be the mid-point of the two QDs. The average coordinate $\langle x \rangle_+$ and $\langle x \rangle_-$ can be written as

$$\langle x \rangle_+ = \langle x \rangle_0 + \tan^2(\Theta/2)\langle x \rangle_1 + 2\tan(\Theta/2)\langle x \rangle_{01} \tag{4}$$

and

$$\langle x \rangle_- = \tan^2(\Theta/2)\,\langle x \rangle_0 + \langle x \rangle_1 - 2\tan(\Theta/2)\langle x \rangle_{10} \tag{5}$$

for the corresponding quasi-doublets within the electron spectrum. Single electron can be localized in one or another QD and $\langle x \rangle_+ \approx \langle x \rangle_0$ and $\langle x \rangle_- \approx \langle x \rangle_1$.

V. RESULTS OF NUMERICAL MODELING

The schematic representation of the 3D geometry of the DQD/QW complex is presented in Fig. 2(a). This complex comprises two quantum dots: a left quantum dot (QD1) and a right quantum dot (QD2). These quantum dots have slightly different sizes, which are designed to simulate a typical experimental situation. Notably, the difference in their radii does not exceed 6%. The quantum dots have a height of 14 nm. The inter-dot distance has been carefully chosen to ensure the uncoupling of the quantum dots if isolated from the QW. The quantum well is separated from the double quantum dot by a specific distance, as shown in Fig. 2(b). This separation creates an energy barrier between them.In the numerical modeling, we transform the Schrödinger equation (1) into an algebraic problem by employing the finite difference method on a mesh. The calculations are performed for two variants of "analyte materials," which differ by the size variations of the corresponding QW. The first variant refers to the situation where the electronic ground state of the "analyte" is lower than the ground state of the DQD. The spectral distribution of delocalized states is expressed by the matrix elements $\langle z \rangle$ of the z-coordinate, which characterizes the spatial localization of the electron along the z axis. The tunneling between the DQD and the analyte is discerned when the value of $\langle z \rangle$ deviates from its "unperturbed" state, which corresponds to the absence of the DQD/analyte coupling. The peaks observed in the spectral distribution $\langle z \rangle$ correspond to specific energy states associated with the isolated DQD. In Fig. 3, the red vertical lines represent the energy levels of the isolated DQD. It serves as a reference to compare and understand the influence of the QW on the DQD energy levels, as shown by the peaks in the spectral distribution. One can see that the electron-delocalized states in the DQD/QW complex correspond to the energy levels of the isolated DQD. The resonance coupling between the DQD and the QW is responsible

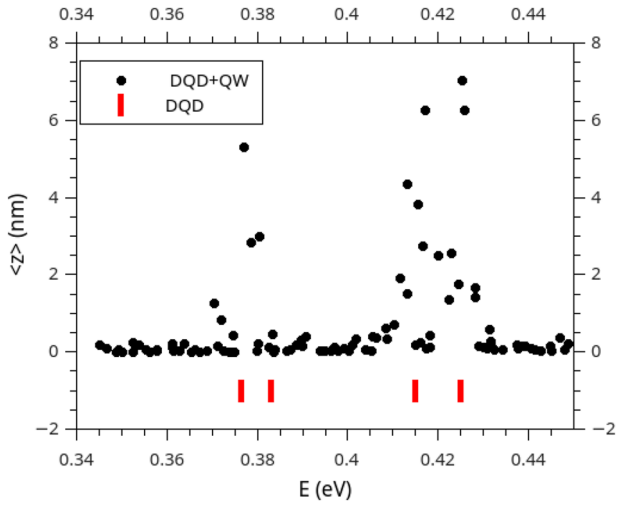

FIG. 3. The tunneling in the DQD/QW complex between QDs and QW (dots): The spectral distribution of delocalized states expressed by the matrix elements $\langle z \rangle$ of z-coordinate. The tunneling is detected when $\langle z \rangle$ is large. The corresponding peaks are related to the isolated DQD levels. The spectrum levels of the isolated DQD are shown by red vertical lines.

for this relationship. Therefore, the mediation of the QW enables the coupling in the DQD. In the isolated DQD, the QDs are uncoupled due to their sufficiently large inter-dot distances and differences in sizes. This corresponds to the situation where $W \approx 0$ [as described by Eq. (3)]. However, in the DQD/QW complex, W takes a non-zero value. Tunneling occurs between the levels of the DQD and the nearby QW levels when the ratio W/Δ is large. Here, Δ represents the energy difference between the electron levels of separated QDs and a single isolated QW.

In Fig. 4(a), we demonstrate the influence of the presence of the DQD on the spectrum of the QW. We compare the spectrum of the isolated QW with that in the DQD/QW complex. Below the ground state of the isolated DQD, the spectra of the isolated QW and the complex are identical. However, above the ground state of the DQD, there is a deviation from the spectrum of the isolated QW. In Fig. 4(b), this deviation is also illustrated by the values of the energy difference $\Delta E = E_{DQD+QW} - E_{QW}$.

The second variant of the QW size corresponds to the situation where the DQD's electronic ground state is lower than the analyte's ground state. The corresponding results of numerical modeling are presented in Figs. 5(a) and 5(b). Figure 5(a) illustrates the tunneling process between quantum dots (QDs) and a quantum well (QW) within the DQD/QW complex. The solid circles represent the QDs and QW. The tunneling refers to the phenomenon where electrons can traverse through the barrier separating the quantum dots and the quantum well. In Fig. 5(b), the tunneling in the QD pair is described using the parameter σ. The σ parameter takes on different values, each corresponding to distinct states: (a) Localized State: For certain values of σ, the electrons remain localized within the individual quantum dots. (b) Parity Delocalized State: Other values of σ

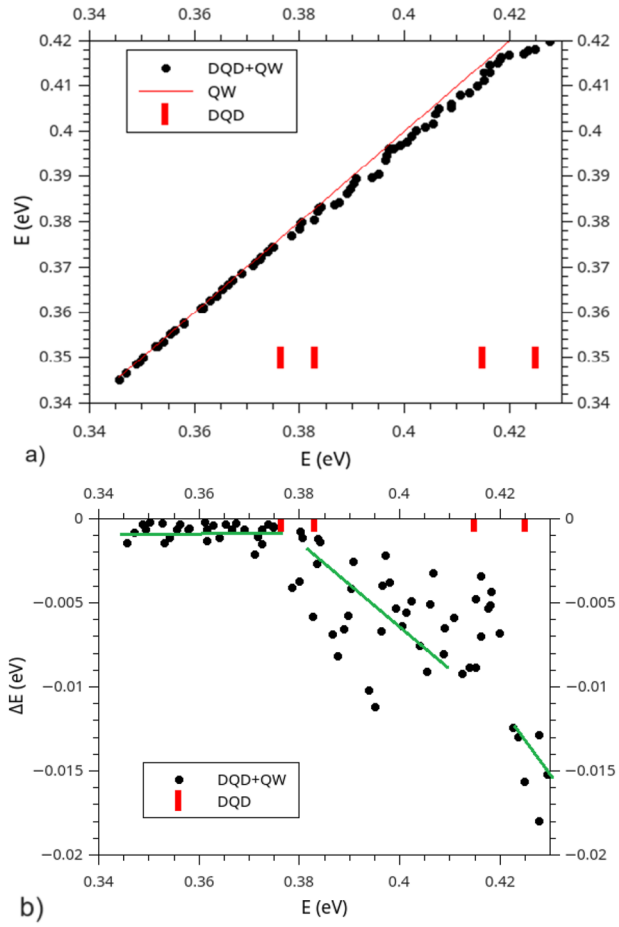

FIG. 4. Influence of DQD on the spectrum of the DQD/QW complex. (a) The spectra of the complex without DQD (red line) and with DQD (solid circles) along the isolated QW spectra. (b) The deviation of energies of the DQD/QW spectral levels from those of the QW spectra $\Delta E = E_{DQD+QW} - E_{QW}$. Spectral positions of the isolated DQD energy levels are shown in red color lines. The unperturbed states of the QW are shown by the horizontal line (in green). A deviation from unperturbed states is shown by the line with an angle.

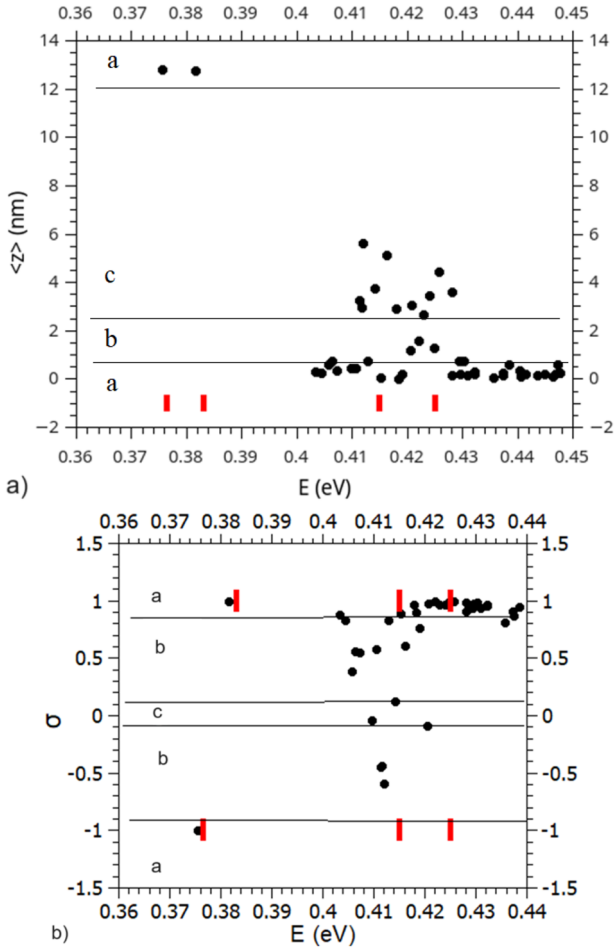

FIG. 5. (a) The tunneling between QDs and QW (solid circles) in the DQD/QW complex. The notations are the same as in Fig. 3. (b) The tunneling in the QD pair is explained by the σ parameter. The values of the parameter correspond to localized (a), parity delocalized (b), and delocalized states (c). The areas of the values are shown by the horizontal lines. The properties of the "analyte" were changed by the parameter V_s from 0.31 eV (in Fig. 3) to 0.37 eV (in the current one). The tunneling in the first quasi-doublet state of DQD is not detected.

lead to parity delocalized states, where electrons are partially shared between the quantum dots. (c) Delocalized State: In some cases, σ values result in fully delocalized states, where electrons are evenly distributed over the entire QD pair. The horizontal lines in the right panel show the different regions of σ values corresponding to the localized, parity-delocalized, and delocalized states. The properties of the "analyte," referring to the substance or system being studied, were altered by changing the parameter V_s from 0.31 to 0.37 eV. It is essential to note that the inter-dot tunneling in the first quasi-doublet state of DQD was not detected. Thus, the first quasi-doublet

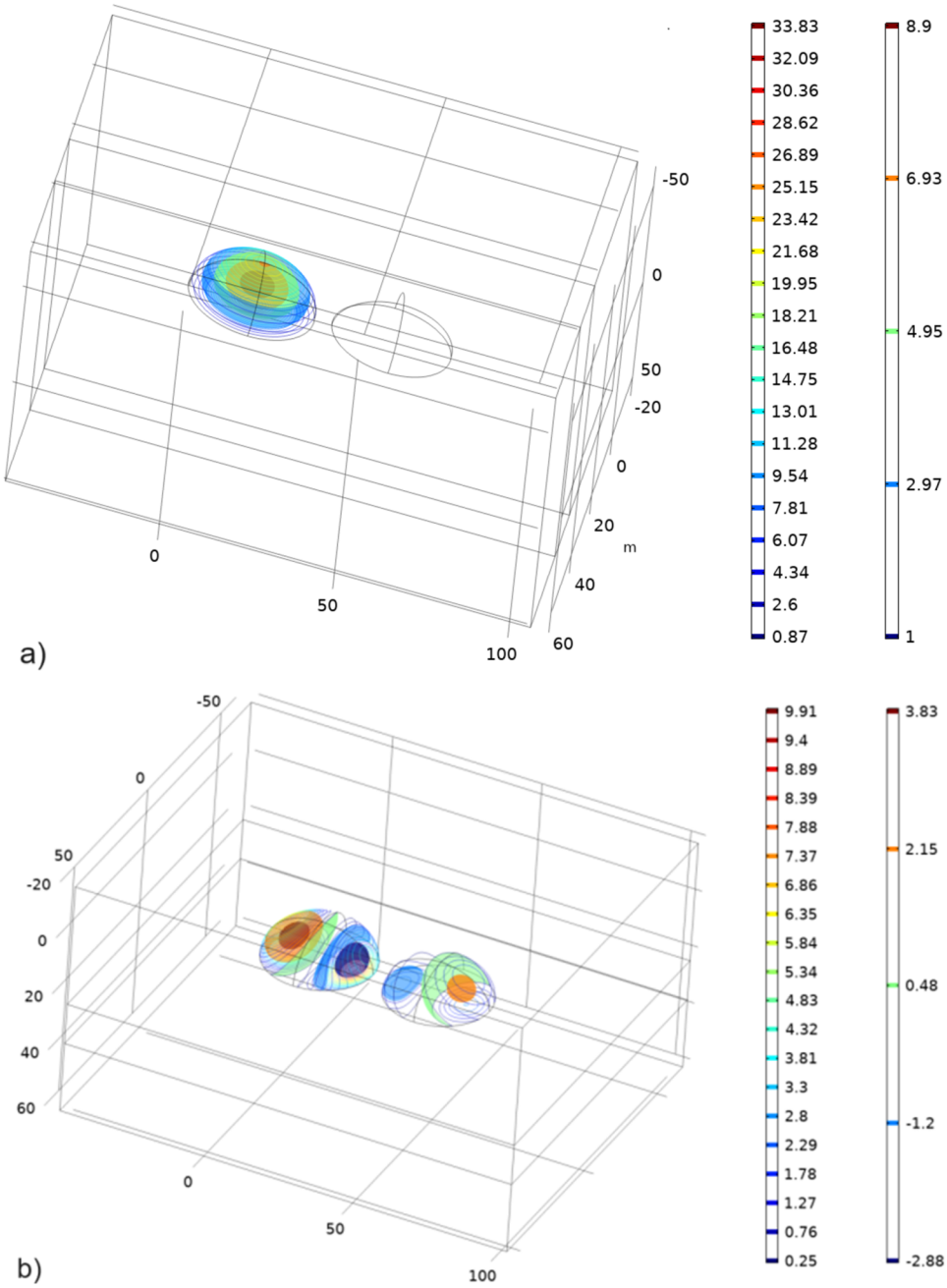

FIG. 6. The isosurface and contour plots depict the electron wave functions for the lowest confinement states of the DQD/QW complex. The remaining portion of the wave function in the QW is not shown. (a) The ground state wave function is localized in the left QD (or in the right QD). No coupling is observed between the two QDs. (b) The electron wave function is delocalized over both QDs in a coupled excited state.

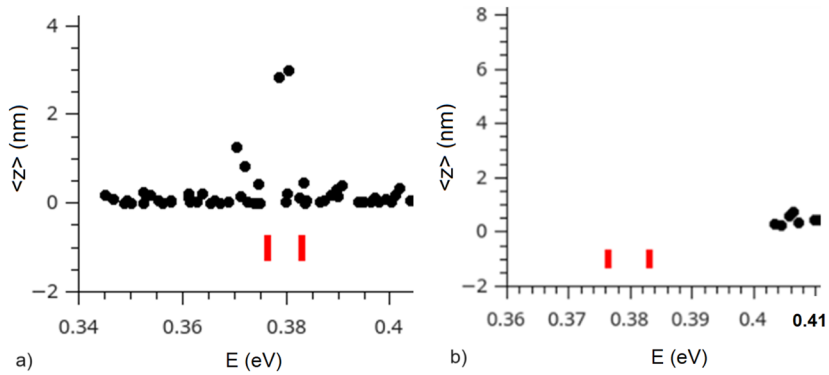

FIG. 7. The binary response (1 or 0) of the two different "analytes": (a) in the ground state of DQD, there is tunneling, and (b) no coupled (tunneling) state is in the ground state of DQD. The notations are the same as in Fig. 3.

of the DQD does not couple with the QW. The electron can be located in left QDs or right QD. Due to the size difference of the QDs, the QDs are uncoupled. This situation is shown in Fig. 6(a) where the isosurface and contour plots depict the electron wave function for the lowest confinement states of the DQD/QW complex. The lower state (lower member) of DQD is unperturbed and is not coupled with the upper member of the quasi-doublet. The next figure [Fig. 6(b)] shows the situation when the electron is delocalized over both QDs. This excited state corresponds to a coupling between DQD and QW. In addition, the QDs in DQD are also coupled.

Detecting electron tunneling between two coupled quantum dots typically involves various experimental techniques. Overall, a combination of these experimental techniques, along with precise device fabrication and control, allows for the detection and characterization of electron tunneling between coupled quantum dots. These methods provide valuable insights into the electronic properties and transport phenomena of such systems, enabling the development of advanced quantum devices and technologies.

VI. DQD-BASED SENSOR

One can propose utilizing the formalism given above for a quantum sensor. We assume to have an array of N detectors, and each detector provides a discrete output value. The detector output, if below the threshold, has assigned a bit value of 0; otherwise, it assigns a bit value of 1. Define a threshold value that determines how the detector outputs are mapped to the bit values. The threshold can be a fixed value, or it can be a dynamic threshold based on the characteristics of the detector and the desired signal representation. Iterate through the detector outputs and compare each output value to the threshold. Assign a bit value of 0 or 1 based on the comparison. Store or process the generated bit signal for further analysis or use. It is important to note that the choice of the threshold will depend on the specific characteristics of the detector and the desired signal representation. One may need to experiment or calibrate the threshold based on the range and distribution of the detector outputs. In addition, one may need to consider any noise, variability, or uncertainties in the detector outputs. Our

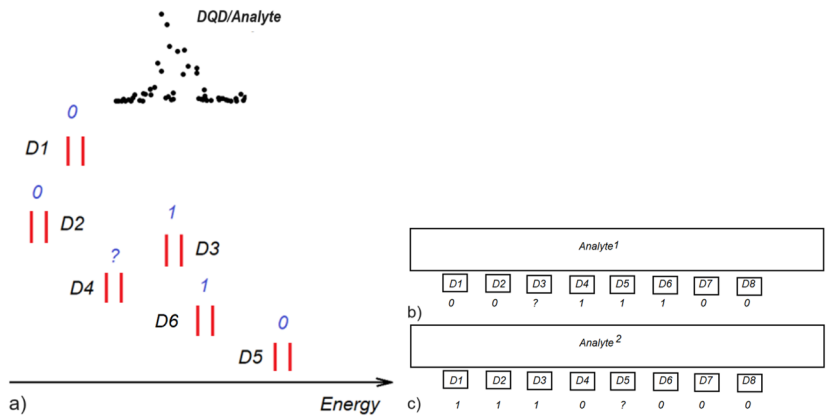

FIG. 8. (a) Generation of signal ("0" or "1" or "?") in detectors (D1. . .D6) in dependence of the ground state DQDs location near resonance low-lying levels of an analyte. The notations are the same as in Fig. 3. The right panel: The representation (schematically) for the detecting of different analytes: two maps of redistricted signals from detectors (D1. . .D8) (b) 0,0,?,1,1,1,0,0 and (c) 1,1,1,0,?,0,0,0. The symbol "?" means an indefinite result of a measurement in the corresponding detector.

proposition for analyte detection is based on the considerations in Sec. V. According to them, the interpretation of the digital signal is presented in Figs. 7(a) and 7(b). In these figures, the binary response of the two different detectors is depicted: (a) a signal of 1 represents tunneling in the ground state of the DQD and (b) a signal of 0 indicates no tunneling in the DQD ground state.

The realistic picture has to include a chaotic distribution of DQD sizes in the array. For example, one can see an example of such DQD arrays produced in the experiments.[33] In the case of six DQDs in detector arrays, Fig. 8 illustrates the detection of low-lying levels of an analyte using a DQD spectrum (a). This scenario generates a signal represented as 0,0,?,1,1,0, (b) where each value corresponds to the output from a specific detector. The symbol "?" denotes an indefinite result of a measurement in the respective detector.

The analyte detection procedure is demonstrated in Fig. 8(c) for eight DQD arrays. The detection process involves comparing the obtained signal with an etalon given by measurements on the same DQD array.

VII. CONCLUSION

Modeled is a double quantum dot/analyte complex and explored its potential for quantum sensing applications. The fundamental concept behind this study is that different analytes, or target molecules, can generate distinct spectral distributions of electron tunneling in the DQD subsystem. By observing and analyzing these unique tunneling patterns, valuable information about the analyte's properties and characteristics can be obtained. Considered is also an array of DQDs in addition to a single DQD structure. The utilization of multiple DQDs offers several advantages, including enhanced sensitivity and the ability to obtain more comprehensive insights into the analyte's spectrum. By incorporating an array of DQDs, we can capture a broader range of tunneling events and gather more detailed data on the interactions between the analyte and the DQD system. In the presented study, we consider DQD based on the InAs/GaAs heterostructure. The effective potential model proposed in Ref. 34 allows us to simplify the consideration and obtain the qualitative results of electron tunneling. The specific assumption of the model is that the analyte spectrum is simulated by employing an InAs/GaAs quantum well in 3D with a quasi-discrete spectrum. The numerical results from modeling efforts highlight the promising capabilities of this DQD/analyte complex for quantum sensing applications. By carefully examining the spectral distributions of electron tunneling, it is possible to identify specific analytes, determine their concentration, and even gather information about their chemical or physical properties. The proposed approach holds significant potential across diverse fields, including chemistry, biology, and materials science, where selective, accurate, and dependable detection and characterization of targeted molecules are paramount.

ACKNOWLEDGMENTS

This work was supported by the DHS Science and Technology Directorate Office of University Programs Summer Research Team Program for Minority Serving Institutions. This research was performed under an appointment to the U.S. Department of Homeland Security (DHS) Science and Technology (S&T) Directorate Office of University Programs Summer Research Team Program for Minority Serving Institutions, administered by the Oak Ridge Institute for Science and Education (ORISE) through an interagency agreement between the U.S. Department of Energy (DOE) and DHS. ORISE is managed by ORAU under DOE Contract No. DE-SC0014664. All opinions expressed in this paper are the author's and do not necessarily reflect the policies and views of DHS, DOE, or ORAU/ORISE. I.F. and B.V. work is partly supported by US National Science Foundation Grant No. HRD-1345219 award and the Department of Energy/National Nuclear Security Administration Award No. NA0003979.

AUTHOR DECLARATIONS

Conflict of Interest

The authors have no conflicts to disclose.

Author Contributions

I. Filikhin: Conceptualization (equal); Investigation (equal); Writing – original draft (equal). **B. Vlahovic**: Conceptualization (equal); Methodology (equal); Project administration (equal); Resources (equal); Writing – review & editing (equal). **A. Joseph**: Investigation (equal); Software (equal). **T. Alston**: Visualization (equal). **J. Oxley**: Conceptualization (equal); Data curation (equal); Formal analysis (equal); Resources (equal); Writing – review & editing (equal).

DATA AVAILABILITY

The data that support the findings of this study are available from the corresponding author upon reasonable request.

REFERENCES

[1] P. Yu *et al.*, "Single-molecule tunneling sensors for nitrobenzene explosives," Anal. Chem. **94**, 12042–12050 (2022).
[2] Y. Miao, J. Lv, Y. Li, and G. Yan, "Construction of biomolecular sensors based on quantum dots," RSC Adv. **6**, 109009 (2016).
[3] Z. Yue *et al.*, "Quantum-dot-based photoelectrochemical sensors for chemical and biological detection," ACS Appl. Mater. Interfaces **5**(8), 2800–2814 (2013).
[4] B. Vlahovic and V. Malloy, "Nanostructure based methods for detection structure determination separation transport extraction and control of chemical and biochemical material," U.S. patent 8,617,469 (December 31, 2013).
[5] B. Vlahovic and V. Malloy, "Detection methods and detection devices based on the quantum confinement effects," U.S. patent 8,262,998 (September 11, 2012).
[6] S. Lian, D. J. Weinberg, R. D. Harris, M. S. Kodaimati, and E. A. Weiss, "Subpicosecond photoinduced hole transfer from a CdS quantum dot to a molecular acceptor bound through an exciton-delocalizing ligand," ACS Nano **10**(6), 6372–6382 (2016).
[7] I. Filikhin, A. Karoui, and B. Vlahovic, "Nanosensing backed by the uncertainty principle," J. Nanotechnol. **2016**, 3794109.
[8] I. Filikhin, T. Peterson, B. Vlahovic, S. P. Kruchinin, Y. B. Kuzmichev, and V. Mitic, "Electron transfer from the barrier in InAs/GaAs quantum dot-well structure," Phys. E **114**, 113629 (2019).
[9] I. Filikhin, A. Karoui, T. Zatezalo, S. P. Kruchinin, and B. Vlahovic, "Effect of double quantum dot asymmetry on electron localization," Mod. Phys. Lett. B (published online 2023).

[10]A. Maiti, J. A. Rodriguez, M. Law, P. Kung, J. McKinney, and P. Yang, "SnO_2 nanoribbons as NO_2 sensors: Insights from first principles calculations," Nano Lett. **3**, 1025–1028 (2003).
[11]R. D. Harris *et al.*, "Electronic processes within quantum dot-molecule complexes," Chem. Rev. **116**, 12865–12919 (2016).
[12]V. Ermakov, S. Kruchinin, T. Pruschke, and J. Freericks, "Thermoelectricity in tunneling nanostructures," Phys. Rev. B **92**, 155431 (2015).
[13]S. Kruchinin and T. Pruschke, "Thermopower for a molecule with vibrational degrees of freedom," Phys. Lett. A **378**, 1157–1161 (2014).
[14]W. A. A. Mohamed, H. Abd El-Gawad, S. Mekkey, H. Galal, H. Handal, H. Mousa, and A. Labib, "Quantum dots synthetization and future prospect applications," Nanotechnol. Rev. **10**, 1926–1940 (2021).
[15]C. Cohen-Tannoudji *et al.*, *Quantum Mechanics*, 12th ed. (Wiley VCH, 2019).
[16]J. Park *et al.*, "Coulomb blockade and the Kondo effect in single-atom transistors," Nature **417**, 722–725 (2002).
[17]M. Sistani *et al.*, "Coulomb blockade in monolithic and monocrystalline Al-Ge-Al nanowire heterostructures," Appl. Phys. Lett. **116**, 013105 (2020).
[18]S. J. An *et al.*, "Impact of the gate geometry on adiabatic charge pumping in InAs double quantum dots," Nanoscale Adv. **4**, 3816 (2022).
[19]S. M. Cronenwett, T. H. Oosterkamp, and L. P. Kouwenhoven, "A tunable Kondo effect in quantum dots," Science **281**, 540–544 (1998).
[20]J. M. Elzerman, R. Hanson, L. H. Willems van Beveren, B. Witkamp, L. M. K. Vandersypen, and L. P. Kouwenhoven, "Single-shot read-out of an individual electron spin in a quantum dot," Nature **430**, 431–435 (2004).
[21]E. Chanrion *et al.*, "Charge detection in an array of CMOS quantum dots," Phys. Rev. Appl. **14**, 024066 (2020).
[22]T. A. Fulton and G. J. Dolan, "Observation of single-electron charging effects in small tunnel junctions," Phys. Rev. Lett. **59**, 109 (1987).
[23]J. P. R. S. Carvalho and S. G. De-Simone, "Electro sensors based on quantum dots and their applications in diagnostic medicine," in *New Advances in Biosensing*, Biomedical Engineering, edited by S. Karakuş (IntechOpen, 2024).
[24]K. Bian, W. Zheng, X. Zeng *et al.*, "Nanoscale electric-field imaging based on a quantum sensor and its charge-state control under ambient condition," Nat. Commun. **12**, 2457 (2021).
[25]A. V. Tsukanov and V. G. Chekmachev, "Electric-field sensor based on a double quantum dot in a microcavity," Semiconductors **51**(9), 1200–1207 (2017).
[26]G. Giavaras, J. Wabnig, B. W. Lovett, J. H. Jefferson, and G. A. D. Briggs, "Magnetic field sensing using a driven double quantum dot," Phys. E **42**, 895–898 (2010).
[27]D. Maradan, L. Casparis, T. M. Liu *et al.*, "GaAs quantum dot thermometry using direct transport and charge sensing," J. Low Temp. Phys. **175**, 784–798 (2014).
[28]S. Su, J. Fan, B. Xue, L. Yuwen, X. Liu, D. Pan, C. Fan, and L. Wang, "DNA-conjugated quantum dot nanoprobe for high-sensitivity fluorescent detection of DNA and micro-RNA," ACS Appl. Mater. Interfaces **6**, 1152–1157 (2014).
[29]J.-B. Li, S. Liang, S. Xiao, M.-D. He, L.-H. Liu, J.-H. Luo, and L.-Q. Chen, "A sensitive biosensor based on optical bistability in a semiconductor quantum dot-DNA nanohybrid," J. Phys. D: Appl. Phys. **52**, 035401 (2019).
[30]C. N. Banwell and E. McCash, *Fundamentals of Molecular Spectroscopy* (McGraw-Hill Education, 1996).
[31]W. Grochala, R. Hoffmann, and P. P. Edwards, "Vibronic coupling in molecules and in solids," Chem. - Eur. J. **9**, 575–587 (2003).
[32]I. B. Bersuker (Ed.), *Electronic Structure and Properties of Transition Metal Compounds: Introduction to the Theory*, 2nd ed. (John Wiley and Sons, Inc, 2010), pp. 324–387.
[33]Y. I. Mazur *et al.*, "Tunneling-barrier controlled excitation transfer in hybrid quantum dot-quantum well nanostructures," J. Appl. Phys. **108**, 074316 (2010).
[34]I. Filikhin, V. M. Suslov, and B. Vlahovic, "Modelling of InAs/GaAs quantum ring capacitance spectroscopy in the non-parabolic approximation," Phys. Rev. B **73**, 205332 (2006).
[35]I. Filikhin, V. M. Suslov, M. Wu, and B. Vlahovic, "InGaAs/GaAs quantum dots within an effective approach," Phys. E **41**, 1358 (2009).
[36]P. W. Atkins and R. S. Friedman, *Molecular Quantum Mechanics* (Oxford University Press Inc., New York, 2005), pp. 168–180.